Static magnetic susceptibility, crystal field and exchange interactions in rare earth titanate pyrochlores

Malkin, B. Z.; Lummen, T. T. A.; van Loosdrecht, P. H. M.; Dhalenne, G.; Zakirov, A. R.

Published in:
Journal of Physics-Condensed Matter

DOI:
10.1088/0953-8984/22/27/276003

Publication date:
2010

J. Phys.: Condens. Matter **22** (2010) 276003 (11pp) doi:10.1088/0953-8984/22/27/276003

Static magnetic susceptibility, crystal field and exchange interactions in rare earth titanate pyrochlores

B Z Malkin[1], T T A Lummen[2,4], P H M van Loosdrecht[2], G Dhalenne[3] and A R Zakirov[1]

[1] Kazan State University, Kazan 420008, Russian Federation
[2] Zernike Institute for Advanced Materials, University of Groningen, 9747 AG Groningen, The Netherlands
[3] Laboratoire de Physico-Chimie de L'Etat Solide, ICMMO, UMR 8182, Université Paris-Sud, 91405 Orsay, France

E-mail: boris.malkin@ksu.ru

Received 21 March 2010, in final form 5 May 2010
Published 23 June 2010
Online at stacks.iop.org/JPhysCM/22/276003

Abstract
The experimental temperature dependence (T = 2–300 K) of single crystal bulk and site susceptibilities of rare earth titanate pyrochlores $R_2Ti_2O_7$ (R = Sm, Eu, Gd, Tb, Dy, Ho, Er, Yb) is analyzed in the framework of crystal field theory and a mean field approximation. Analytical expressions for the site and bulk susceptibilities of the pyrochlore lattice are derived taking into account long range dipole–dipole interactions and anisotropic exchange interactions between the nearest neighbor rare earth ions. The sets of crystal field parameters and anisotropic exchange coupling constants have been determined and their variations along the lanthanide series are discussed.

(Some figures in this article are in colour only in the electronic version)

1. Introduction

Magnetic properties of crystals containing rare earth ions residing on a network of corner sharing tetrahedra (pyrochlore lattice) have been extensively studied during recent years. The pyrochlore lattice belongs to the class of geometrically frustrated systems where interactions between magnetic ions cannot be minimized simultaneously. The rare earth titanates $R_2Ti_2O_7$ with the cubic $Fd\bar{3}m$ space group have such an arrangement of rare earth ions, R^{3+} [1], and, as a consequence of the geometric frustration, exhibit a large variety of intriguing equilibrium and dynamic magnetic properties (for a review see [2]). Rather specific magnetic structures of the ordered states in $Gd_2Ti_2O_7$ and $Er_2Ti_2O_7$, spin ice properties of $Dy_2Ti_2O_7$ and $Ho_2Ti_2O_7$, spin liquid behavior of $Tb_2Ti_2O_7$ and the first order transition of spin dynamics in $Yb_2Ti_2O_7$ have been discovered so far. To better understand these exotic magnetic properties, i.e. the time and space dependencies of spin correlations, knowledge of microscopic mechanisms of interactions between paramagnetic ions is of primary importance.

Measurement of the dc-magnetic susceptibility (determined as a ratio of the induced magnetization to the corresponding weak external magnetic field) is a conventional tool to obtain information about the electronic structure of a magnetic system and of the magnetic interactions between paramagnetic ions. The temperature dependence of the isotropic susceptibilities of polycrystalline and single crystals of rare earth titanates have been presented in a number of recent publications (R = Sm [3], Eu [4], Gd [5–10], Tb [8–16], Dy [8, 9, 17–20], Ho [8, 9, 11, 20–23], Er [8, 11, 18, 24], Yb [8, 11, 17, 18, 25, 26]). As a rule, the experimental data were analyzed using the Curie–Weiss law leading to estimations of the effective isotropic exchange coupling constant. Recently, the temperature dependence of the anisotropic site susceptibilities of R^{3+} ions in $R_2Ti_2O_7$ (R = Tb, Ho, Er, Yb) were measured using polarized neutron diffraction experiments. These experimental results were interpreted

[4] Present address: Pennsylvania State University, 254 MRL building, University Park, PA 16802, USA.

within the framework of a crystal field theory and a mean field approximation by introducing effective anisotropic molecular field tensors [27].

Despite a number of published theoretical and experimental studies of the magnetic susceptibility of rare earth compounds with the pyrochlore structure, the exact relation between the bulk (macroscopic) and single ion (microscopic) susceptibilities, that should account for dipolar and exchange interactions between the rare earth ions, has not been presented in the literature. In section 2 of the present paper, we derive such a relation in the framework of a single site mean field approximation. To facilitate a detailed comparison of the results of calculations with experimental data, the dc-susceptibility of single crystalline Tb, Ho, Gd and Dy titanate was measured in the temperature range 2–300 K (section 3). Anisotropic single ion susceptibilities were computed using sets of crystal field parameters (CFP) obtained from calculations in the framework of the exchange charge model [28] and from a systematic analysis of the available data on spectral and magnetic properties of rare earth titanate pyrochlores. Parameters of the anisotropic exchange interaction between the nearest neighbor R^{3+} (R = Gd, Tb, Dy, Ho, Er) ions have been determined through fitting the calculated bulk and site susceptibilities (section 4) to the experimental data. Conclusions are given in section 5.

2. Theoretical background

The pyrochlore lattice has a rhombohedral primitive unit cell with translation vectors $\boldsymbol{a}_1 = a(1/2\ 1/2\ 0)$, $\boldsymbol{a}_2 = a(1/2\ 0\ 1/2)$, $\boldsymbol{a}_3 = a(0\ 1/2\ 1/2)$ and contains four magnetically nonequivalent face-centered R-sublattices with the basis vectors $\boldsymbol{r}_1 = a(111)/8$, $\boldsymbol{r}_2 = a(\bar{1}\ \bar{1}\ 1)/8$, $\boldsymbol{r}_3 = a(\bar{1}\ 1\ \bar{1})/8$ and $\boldsymbol{r}_4 = a(1\ \bar{1}\ \bar{1})/8$, where a is the lattice constant which varies approximately linearly with the ionic radius of the R-ion (at room temperature $a = 1.020\,56$ nm (R = Sm); $a = 1.003\,25$ nm (R = Yb)) [1]. The point symmetry group at the R-site is D_{3d}, the trigonal symmetry axis is oriented along the corresponding basis vector. In this section, we consider a linear response of the R-sublattice to the external magnetic field $\boldsymbol{B}$.

In the absence of an external field, the Hamiltonian of rare earth ions in a crystal has the following form:

$$H = \sum_{Kn} H_s(Kn) + \tfrac{1}{2} \sum_{KnK'n'} \boldsymbol{m}(Kn)\boldsymbol{\Lambda}(Kn, K'n')\boldsymbol{m}(K'n'). \tag{1}$$

Here $H_s(Kn)$ is the Hamiltonian of an ion in the unit cell K belonging to the sublattice n with the magnetic moment operator $\boldsymbol{m}\ (Kn)$, the second term corresponds to magnetic interactions between ions. The magnetic moment operator of a rare earth ion is given by the expression $\boldsymbol{m} = \mu_B \sum (\boldsymbol{l} + 2\boldsymbol{s})$, where the sum is taken over 4f electrons with the orbital momentum operator $\boldsymbol{l}$ and spin operator $\boldsymbol{s}$, μ_B is the Bohr magneton. In the framework of the mean field approximation, the effective Hamiltonian of a single ion can be written as

$$H_{\mathrm{eff,s}}(Kn) = H_0(Kn) + H_{\mathrm{CF}}(Kn) - \boldsymbol{m}(Kn)\boldsymbol{B}_n^{(l)}, \tag{2}$$

where H_0 is the Hamiltonian of a free ion, $\boldsymbol{B}_n^{(l)}$ is the internal local magnetic field. The crystal field Hamiltonian $H_{\mathrm{CF}}(Kn)$ for the ground $4f^N$ electronic configuration of rare earth ions in the pyrochlore lattice is determined by six real CFP B_p^q. In the local Cartesian system of coordinates with the Z_n axis along the corresponding crystal ternary axis and the local X_n axis in the plane containing the crystal z-axis and the basis vector $\boldsymbol{r}_n$, the crystal field Hamiltonian reads

$$H_{\mathrm{CF}} = B_0^2 C_0^{(2)} + B_0^4 C_0^{(4)} + B_0^6 C_0^{(6)} + B_3^4 (C_3^{(4)} - C_{-3}^{(4)}) + B_3^6 (C_3^{(6)} - C_{-3}^{(6)}) + B_6^6 (C_6^{(6)} + C_{-6}^{(6)}) \tag{3}$$

with $C_q^{(p)}$ the spherical tensor operators of rank p. In the presence of an external magnetic field $\boldsymbol{B}$, the local magnetic field introduced in equation (2) equals

$$\boldsymbol{B}_n^{(l)} = \boldsymbol{B} - \sum_{K'n'} \boldsymbol{\Lambda}(0n, K'n')\langle \boldsymbol{m}(n')\rangle, \tag{4}$$

where the brackets $\langle \cdots \rangle$ indicate thermal averaging with the Hamiltonian (2). The tensor $\boldsymbol{\Lambda}$ contains two terms corresponding to magnetic dipole–dipole ($\boldsymbol{\Lambda}^{(\mathrm{dip})}$) and exchange ($\boldsymbol{\Lambda}^{(\mathrm{ex})}$) interactions approximated by bilinear forms of magnetic moments of the nearest neighbor rare earth ions at the distance $r_{nn} = a\sqrt{2}/4 \sim 0.36$ nm. The dipolar contribution equals

$$\Lambda_{\alpha\beta}^{(\mathrm{dip})}(Kn, K'n') = \frac{1}{r_{Kn,K'n'}^3}[\delta_{\alpha\beta} - 3\eta_\alpha(Kn, K'n')\eta_\beta(Kn, K'n')], \tag{5}$$

where $\delta_{\alpha\beta}$ is the Kronecker delta, α and β refer to the x, y, z Cartesian components of $\boldsymbol{B}^{(l)}$ and $\langle \boldsymbol{m}\rangle$, and $\boldsymbol{r}_{Kn,K'n'}$ is the vector connecting two ions with the directional cosines $\eta_\alpha(Kn, K'n')$. According to the crystal lattice symmetry, the tensor $\boldsymbol{\Lambda}^{(\mathrm{ex})}$ can be defined by three independent elements which couple the magnetic moment components along ($\lambda_\parallel$) and normal ($\lambda_{\perp,1}, \lambda_{\perp,2}$) to the bond direction, respectively. In particular, the Hamiltonian of the exchange interaction between the nearest neighbor rare earth ions belonging to the first and second sublattices can be written as (in this case there are two superexchange paths which involve the common nearest neighbor oxygen ions shifted along the crystallographic [001] axis by ∼0.17 nm and ∼−0.13 nm, respectively, from the middle of the bond vector $\boldsymbol{r}_{1,2} = a(1, 1, 0)/4$)

$$H_{\mathrm{exch}}(1, 2) = -\lambda_\parallel m_{z'}(1)m_{z'}(2) - \lambda_{\perp,1} m_{x'}(1)m_{x'}(2) - \lambda_{\perp,2} m_{y'}(1)m_{y'}(2), \tag{6}$$

here the z'-axis is parallel to the bond vector $\boldsymbol{r}_{1,2}$, $\boldsymbol{x}' \parallel [001]$, $\boldsymbol{y}' \parallel [1, -1, 0]$. Now we can present the local magnetic field (equation (4)) in the following form:

$$\begin{aligned}\boldsymbol{B}_n^{(l)} = {} & \boldsymbol{B} - \boldsymbol{B}_d + \sum_{n'} \boldsymbol{Q}(n, n')\langle \boldsymbol{m}(n')\rangle \\ & + \lambda_\parallel \sum_p (\boldsymbol{r}_{n,n'(p)}^- \cdot \langle \boldsymbol{m}(n'(p))\rangle)\boldsymbol{r}_{n,n'(p)}^-/(\boldsymbol{r}_{n,n'(p)}^-)^2 \\ & + \lambda_{\perp,1} \sum_p (\boldsymbol{r}_{n,n'(p)}^+ \cdot \langle \boldsymbol{m}(n'(p))\rangle)\boldsymbol{r}_{n,n'(p)}^+/(\boldsymbol{r}_{n,n'(p)}^+)^2 \\ & + \lambda_{\perp,2} \sum_p (\boldsymbol{R}_{n,n'(p)} \cdot \langle \boldsymbol{m}(n'(p))\rangle)\boldsymbol{R}_{n,n'(p)}/(\boldsymbol{R}_{n,n'(p)})^2,\end{aligned} \tag{7}$$

where the six R^{3+} ions nearest to the R^{3+} ion at the site ($K = 0$, n) are labeled by the index p, $\boldsymbol{r}_{n'(p)}$ is the basis vector of the corresponding sublattice, $\boldsymbol{r}^{\pm}_{n,n'(p)} = \boldsymbol{r}_n \pm \boldsymbol{r}_{n'(p)}$, $\boldsymbol{R}_{n,n'(p)} = \boldsymbol{r}_n \times \boldsymbol{r}_{n'(p)}$, $\boldsymbol{B}_\mathrm{d}$ is the demagnetizing field, and the components of the tensor $\boldsymbol{Q}$ are the corresponding dipole lattice sums (Lorentz factors). These sums were computed by the Ewald method in the crystallographic system of coordinates, in particular, the nonzero components of the tensors $\boldsymbol{Q}(n,n)$ and $\boldsymbol{Q}(1,2)$ equal: $Q_{\alpha\beta}(n,n) = \delta_{\alpha\beta}$, $Q_{xx}(1,2) = Q_{yy}(1,2) = 2.0346$, $Q_{xy}(1,2) = 3.4522$, $Q_{zz}(1,2) = -1.0692$ (in units of $4\pi/3v$, $v = a^3/4$ is the unit cell volume). Below we assume that a sample has an ellipsoid shape with one of its principal axes along the external magnetic field. In this case the demagnetizing field is:

$$\boldsymbol{B}_\mathrm{d} = \frac{4\pi N}{3vB^2}\sum_n (\langle \boldsymbol{m}(n)\rangle \cdot \boldsymbol{B})\boldsymbol{B}, \tag{8}$$

where N is the corresponding demagnetizing factor, which for a spherical sample equals unity.

The single ion susceptibility tensor $\boldsymbol{\chi}^\mathrm{s}$ is diagonal in the local system of coordinates. Components of average magnetic moments equal (k_B is the Boltzmann constant)

$$\langle m(n)_Z\rangle = \frac{\mathrm{Tr}[m_Z \exp(-H_{\mathrm{eff,s}}(n)/k_\mathrm{B}T)]}{\mathrm{Tr}[\exp(-H_{\mathrm{eff,s}}(n)/k_\mathrm{B}T)]} = \chi^\mathrm{s}_\parallel B^{(\mathrm{l})}_{n,Z}, \tag{9}$$

$$\langle m(n)_X\rangle = \chi^\mathrm{s}_\perp B^{(\mathrm{l})}_{n,X}, \qquad \langle m(n)_Y\rangle = \chi^\mathrm{s}_\perp B^{(\mathrm{l})}_{n,Y} \tag{10}$$

(here and below we drop the sublattice subscript for local coordinate axes). To obtain the explicit relation between the bulk and single ion susceptibilities, let us assume that the magnetic field $\boldsymbol{B}$ is parallel to the crystallographic z-axis, the symmetry axis of fourth order. In this case, there are only two independent variables, $\langle m(n)_Z\rangle = \langle m_Z\rangle$ and $\langle m(n)_X\rangle = \langle m_X\rangle$ ($\langle m(n)_Y\rangle = 0$). The components of single ion magnetic moments in the crystallographic frame equal $\langle m(n)_z\rangle = (\langle m_Z\rangle + \sqrt{2}\langle m_X\rangle)/\sqrt{3}$; $\langle m(1)_x\rangle = \langle m(1)_y\rangle = -\langle m(2)_x\rangle = -\langle m(2)_y\rangle = \langle m(3)_x\rangle = -\langle m(3)_y\rangle = -\langle m(4)_x\rangle = \langle m(4)_y\rangle = (\sqrt{2}\langle m_Z\rangle - \langle m_X\rangle)/\sqrt{6}$. Taking into account exchange interactions of each ion with its six nearest neighbors, we obtain components of the local magnetic fields from equation (7). In particular,

$$B^{(\mathrm{l})}_{nz} = B + \frac{2}{\sqrt{3}}\left[\left(\lambda_\parallel + \lambda_{\perp,1} + \lambda_{\perp,2} + \frac{8\pi}{3v}(1-N)\right)(\langle m_Z\rangle + \sqrt{2}\langle m_X\rangle) + (\lambda_\parallel - \lambda_{\perp,2} + q)\left(\langle m_Z\rangle - \frac{1}{\sqrt{2}}\langle m_X\rangle\right)\right], \tag{11}$$

$$B^{(\mathrm{l})}_{1x} = B^{(\mathrm{l})}_{1y} = \frac{1}{\sqrt{3}}\left[(-\lambda_\parallel - 2\lambda_{\perp,1} + \lambda_{\perp,2} - p) \times \left(\langle m_Z\rangle - \frac{1}{\sqrt{2}}\langle m_X\rangle\right) + (\lambda_\parallel - \lambda_{\perp,2} + q) \times (\langle m_Z\rangle + \sqrt{2}\langle m_X\rangle)\right], \tag{12}$$

here $q = Q_{xy}(1,2)$ and $p = Q_{xy}(1,2) + Q_{zz}(1,2) - Q_{zz}(1,1) = 1.383(4\pi/3v)$. Components of the local field affecting ions at the sites of the sublattice $n = 1$ in the local frame equal $B^{(\mathrm{l})}_{1Z} = (B^{(\mathrm{l})}_{1z} + 2B^{(\mathrm{l})}_{1x})/\sqrt{3}$, $B^{(\mathrm{l})}_{1X} = \sqrt{2}(B^{(\mathrm{l})}_{1z} - B^{(\mathrm{l})}_{1x})/\sqrt{3}$. Now, using the definitions (9) and (10) of the single ion susceptibilities, we obtain a system of two coupled self-consistent linear equations relating $\langle m_Z\rangle$ and $\langle m_X\rangle$:

$$\langle m_Z\rangle = \chi^\mathrm{s}_\parallel\left[\frac{1}{\sqrt{3}}B + A\langle m_Z\rangle + \sqrt{2}D\langle m_X\rangle\right], \tag{13}$$

$$\langle m_X\rangle = \chi^\mathrm{s}_\perp\left[\frac{\sqrt{2}}{\sqrt{3}}B + \sqrt{2}D\langle m_Z\rangle + F\langle m_X\rangle\right], \tag{14}$$

where

$$A = \frac{2}{3}\left[2\lambda_\parallel - \lambda_{\perp,1} + 2q - p + \frac{8\pi}{3v}(1-N)\right], \tag{15}$$

$$D = \frac{1}{3}\left[4(\lambda_\parallel + \lambda_{\perp,1}) + q + p + \frac{16\pi}{3v}(1-N)\right], \tag{16}$$

$$F = \frac{1}{3}\left[2\lambda_{\perp,1} + 9\lambda_{\perp,2} - \lambda_\parallel - 4q - p + \frac{32\pi}{3v}(1-N)\right]. \tag{17}$$

The expressions for effective single ion longitudinal and transversal susceptibilities are easily obtained from equations (13) and (14):

$$\chi_\parallel = \frac{\langle m(n)_Z\rangle}{B}\sqrt{3} = \frac{\chi^\mathrm{s}_\parallel}{\Delta}[1 + (3\lambda_\parallel + 2\lambda_{\perp,1} - 3\lambda_{\perp,2} + 2q + p)\chi^\mathrm{s}_\perp], \tag{18}$$

$$\chi_\perp = \frac{\langle m(n)_X\rangle}{B}\sqrt{\frac{3}{2}} = \frac{\chi^\mathrm{s}_\perp}{\Delta}[1 + (2\lambda_{\perp,1} + p - q)\chi^\mathrm{s}_\parallel], \tag{19}$$

where

$$\Delta = 1 - A\chi^\mathrm{s}_\parallel - F\chi^\mathrm{s}_\perp + \chi^\mathrm{s}_\parallel\chi^\mathrm{s}_\perp(AF - 2D^2). \tag{20}$$

The isotropic bulk susceptibility (per R-mole) equals

$$\chi = \frac{\langle m(n)_z\rangle}{B}N_\mathrm{A} = \frac{N_\mathrm{A}}{3}(\chi_\parallel + 2\chi_\perp) = \frac{N_\mathrm{A}}{3\Delta}[\chi^\mathrm{s}_\parallel + 2\chi^\mathrm{s}_\perp + 3(\lambda_\parallel + 2\lambda_{\perp,1} - \lambda_{\perp,2} + p)\chi^\mathrm{s}_\parallel\chi^\mathrm{s}_\perp], \tag{21}$$

where N_A is the Avogadro number. Expression (21) generalizes the result derived in [29].

We can simplify the expression (21) for the case of high temperatures, when the thermal excitation energy $k_\mathrm{B}T$ is much higher than the total crystal field splitting of the ground multiplet of a rare earth ion with the total angular momentum J and the Lande factor g_J. In this case single ion susceptibilities equal [30] $\chi^\mathrm{s}_{\alpha\alpha} = \mathrm{Tr}[m^2_\alpha(1 - H_\mathrm{CF}/k_\mathrm{B}T)]/[(2J+1)k_\mathrm{B}T] + \mathrm{O}(1/T^3)$. Substituting χ^s_{ZZ} and χ^s_{XX} for $\chi^\mathrm{s}_\parallel$ and $\chi^\mathrm{s}_\perp$, respectively, in equations (20) and (21), and taking into account the identities $\mathrm{Tr}H_\mathrm{CF} = 0$, $m^2_X + m^2_Y + m^2_Z = \mu^2_\mathrm{eff} = (g_J\mu_\mathrm{B})^2 J(J+1)$, we obtain the bulk susceptibility

$$\chi = N_\mathrm{A}\frac{C}{T} \times \frac{[1 + (\lambda_\parallel + 2\lambda_{\perp,1} - \lambda_{\perp,2} + p)\frac{C}{T} + \mathrm{O}(1/T^2)]}{[1 - (\lambda_\parallel + 3\lambda_{\perp,2} - p + \frac{16\pi}{3v}(1-N))\frac{C}{T} + \mathrm{O}(1/T^2)]}, \tag{22}$$

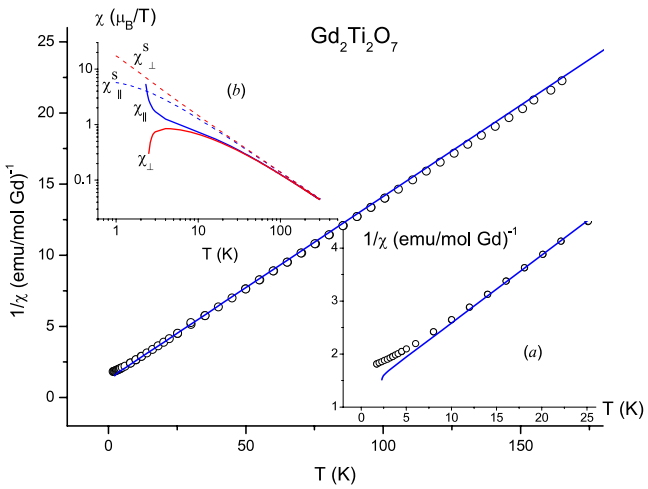

Figure 1. Measured (symbols) and calculated (solid curve) inverse bulk susceptibility of $Gd_2Ti_2O_7$. Inset (*a*) shows the data below 25 K. Inset (*b*): calculated components of the single ion (dashed curves) and the renormalized site susceptibility (solid curves) tensors.

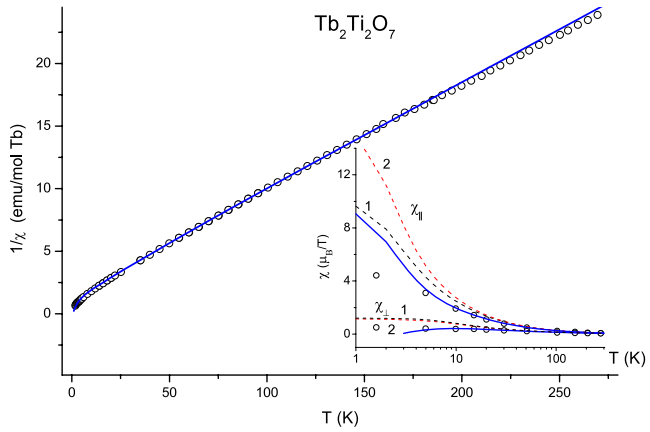

Figure 2. Measured (symbols) and calculated (solid curve) inverse bulk susceptibility in $Tb_2Ti_2O_7$ single crystal (the disk with the demagnetizing factor $N = 1.92$). Inset: site susceptibilities measured in [27] (symbols) and calculated single ion susceptibilities in the crystal field (dotted curves 1), renormalized susceptibilities due to dipole–dipole interactions (dotted curves 2) and due to dipole–dipole and anisotropic exchange interactions (solid curves).

where $C = \mu_{\rm eff}^2/3k_{\rm B}$ is the Curie constant. Up to terms of the second order in $(1/T)$, this expression corresponds to the Curie–Weiss law $\chi = N_{\rm A}\frac{C}{T-\theta_{\rm W}}$, where $\theta_{\rm W} = \theta_{\rm W,ex} + \theta_{\rm W,dip}$ is the Weiss temperature, and

$$\theta_{\rm W,dip} = \frac{\mu_{\rm eff}^2}{3k_{\rm B}}\frac{16\pi(1-N)}{3v}, \tag{23}$$

$$\theta_{\rm W,ex} = \frac{2\mu_{\rm eff}^2}{3k_{\rm B}}(\lambda_{\parallel} + \lambda_{\perp,1} + \lambda_{\perp,2}). \tag{24}$$

The expression for the dipolar contribution $\theta_{\rm W,dip}$ to the Weiss temperature agrees with the result obtained in [12]. Note that the exchange contribution to the Weiss temperature (24) depends only on the 'isotropic' combination of exchange constants $\lambda_{\rm is} = (\lambda_{\parallel} + \lambda_{\perp,1} + \lambda_{\perp,2})/3$.

According to equation (21), the bulk susceptibility, as well as the renormalized single ion susceptibilities $\chi_{\parallel}$ and $\chi_{\perp}$, diverges when the denominator Δ (see equation (20)) equals zero. This divergence signals the possibility of magnetic ordering at low temperatures. However, it is well known that the mean field approximation fails at low temperatures when the energies of thermal excitations $k_{\rm B}T$ become comparable to the energies of magnetic interactions between paramagnetic ions. The magnetic ordering can be destroyed by quantum spin fluctuations (see the review [2] and references therein), by random crystal fields due to crystallographic inhomogeneities, by hyperfine interactions between 4f electrons and the nuclear magnetic moment of a rare earth ion [31] or by quadrupole or pseudo-quadrupole (induced by the virtual phonon exchange) interactions between rare earth ions [32].

3. Experimental results

Magnetic susceptibilities were measured in the temperature range from 2 to 300 K using a Quantum Design MPMS magnetometer equipped with a superconducting quantum interference device (SQUID). Samples were prepared by cutting discs of approximately 5 mm ($Dy_2Ti_2O_7$, $Ho_2Ti_2O_7$) or 4 mm ($Gd_2Ti_2O_7$, $Tb_2Ti_2O_7$) diameter and 1 mm thickness from single crystals grown using the floating zone technique (see [9] for details), which were subsequently placed in a gelcap and fixed in position. The Dy and Ho samples were mounted such that the applied magnetic field of 0.05 T was in the plane of the discs, while the Gd and Tb samples were oriented such that the applied field, 0.01 T in these cases, was normal to the disc plane. Following zero-field cooling down to 2 K, each sample's magnetic susceptibility was measured as a function of increasing temperature. The corresponding demagnetizing factors $N = 0.46$ (Dy, Ho samples) and 1.92 (Gd, Tb samples) were estimated using the calculated values of N for cylindrical samples [33] (the relative errors in the values of dipolar contributions to the Weiss temperature introduced by assuming a uniform demagnetizing field in the discs do not exceed 10% [34]).

The results of measurements are presented in figures 1–4. Our data are in good agreement with the previous work [8] but do not match exactly the obtained earlier temperature dependencies. This is most likely due to variations in the shape of the samples used in previous studies, which were not defined in the most of the previous publications.

4. Discussion

We analyzed the results of our measurements as well as the earlier published data on dc-susceptibilities and optical spectra of rare earth titanate pyrochlores by fitting the crystal field and exchange interaction parameters. The temperature dependence of the single ion susceptibilities $\chi_{\parallel}^{\rm s}$ and $\chi_{\perp}^{\rm s}$ was computed according to definitions (9) and (10). The electrostatic, spin–orbit, electrostatic configuration and correlated spin–orbit and spin–spin interactions were accounted for in the free ion Hamiltonian H_0, the corresponding parameters F^n, ζ, α, β, γ, T^k, P^n, M^n were taken from the literature [35]. The

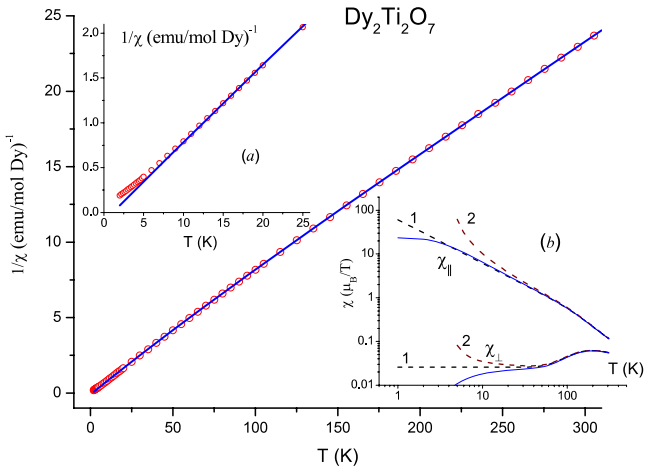

Figure 3. Measured (symbols) and calculated (solid curves) inverse bulk susceptibility of $Dy_2Ti_2O_7$. Inset (*a*) shows the data below 20 K. Inset (*b*)—calculated components of the site susceptibility tensor (dotted curves 1—single ion susceptibilities in the crystal field, dotted curves 2 and solid curves—renormalized susceptibilities due to dipole and dipole + exchange interactions, respectively).

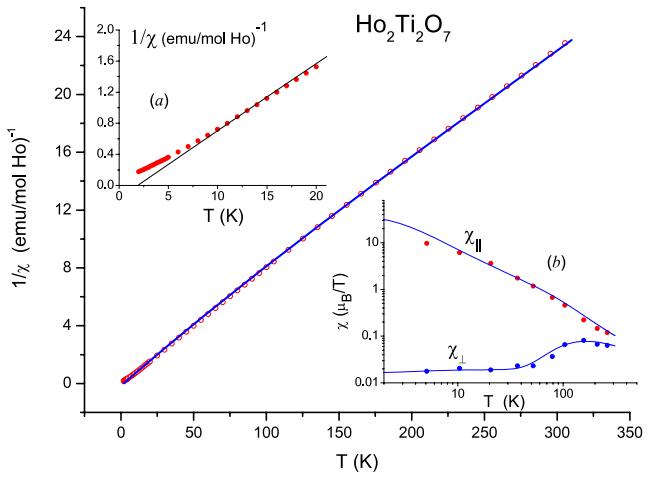

Figure 4. Measured (symbols) and calculated (solid curves) inverse bulk susceptibility of $Ho_2Ti_2O_7$. Inset (*a*) shows the data below 20 K. Inset (*b*)—measured in [27] (symbols) and calculated components of the site susceptibility tensor.

Table 1. Crystal field parameters (in units of cm^{-1}) for $R_2Ti_2O_7$.

	R					
B_p^q	Sm	Eu	Tb[a]	Dy	Ho	Er
B_0^2	230	400	438 (528)	412	539	635
B_0^4	2985	2790	2555 (2155)	2470	2440	2400
B_3^4	785	750	740 (821)	730	716	685
B_0^6	700	800	842 (710)	810	805	762
B_3^6	−630	−650	−630 (−638)	−600	−618	−460
B_6^6	1000	920	820 (788)	830	838	720

[a] Data in brackets correspond to $Tb_2Sn_2O_7$.

sets of CFP used in calculations are presented in table 1. Earlier the CFP for rare earth titanates were estimated in the framework of the exchange charge model [28]. In the present work, the results of these calculations have been corrected to fit the available spectral data and the measured temperature dependence of the dc-susceptibilities. The crystal field energy levels of non-Kramers ions (Eu^{3+}, Tb^{3+}, Ho^{3+}) are classified below according to irreducible representations A_1, A_2 (singlets) and E (doublets with g-factors $g_\parallel \neq 0$, $g_\perp = 0$) of the D_{3d} symmetry group, doublet states of Kramers ions (Sm^{3+}, Gd^{3+}, Dy^{3+}, Er^{3+}, Yb^{3+}) with the odd number of 4f electrons correspond to irreducible representations Γ_4 ($g_\parallel \neq 0$, $g_\perp \neq 0$) and Γ_{56} ($g_\parallel \neq 0$, $g_\perp = 0$). Each system containing rare earth ions with the ground electronic configuration $4f^N$ ($N = 5{:}13$) is considered separately below. We begin from the analysis of the experimental data obtained in the current work and then we discuss the literature data for the Sm, Eu, Er and Yb titanates.

4.1. $Gd_2Ti_2O_7$

The ground state $^8S_{7/2}$ of the free Gd^{3+} ion is split into four doublets in the crystal field of D_{3d} symmetry. Since we expect a monotonous variation of the CFP along the lanthanide series in isomorphic compounds, we have estimated the CFP for the Gd^{3+} ions with the $4f^7$ configuration as average values of the CFP for the $4f^6$ and $4f^8$ configurations in Eu and Tb titanates (see table 1), respectively. Numerical diagonalization of the Hamiltonian $H_0 + H_{CF}$ operating in the Hilbert space of the $4f^7$ configuration brings a total splitting of 0.5 cm^{-1} for the $^8S_{7/2}$ state that is about half that of the measured value of this splitting in the diluted system $Y_2Ti_2O_7$:Gd [36]. More important is the fact that the obtained easy axis anisotropy contradicts the results of EPR studies [36]. It is highly plausible that charge transfer effects and configuration interactions should be taken into account explicitly to describe correctly the magnetic properties of S-state ions. In the present work, to calculate single ion susceptibilities, we used a semi-phenomenological approach based on the introduction of the effective spin-Hamiltonian operating in the space of the spin $S = 7/2$ wavefunctions. The parameters of the spin-Hamiltonian were determined in [36].

The temperature dependence of the single crystal susceptibility measured in the present work (see figure 1) agrees qualitatively with the data for the polycrystalline samples published earlier [5, 6]. At high temperatures, $T >$ 10 K, the bulk susceptibility is described by the Curie–Weiss law. The measured Weiss temperature for the single crystal, $\theta_W = -10.3$ K, is close to values of −9.4 K [6], −9.6 K [5], −9.9 K [7] found earlier for polycrystalline samples.

Because only the ground multiplet $^8S_{7/2}$ with the zero orbital moment is populated at any physically meaningful temperature, we have good reasons to assume the isotropic Heisenberg exchange interaction $H_{exch} = -J\boldsymbol{S}_1\boldsymbol{S}_2$ for the nearest neighbor Gd^{3+} ions. According to definition (6), in this case $\lambda_\parallel = \lambda_{\perp,1} = \lambda_{\perp,2} = \lambda_{is}$, and the exchange coupling constant equals $J = (2\mu_B)^2\lambda_{is}$. For the sample studied, the calculated dipolar contribution $\theta_{W,dip}$ into the Weiss temperature equals −0.763 K, and thus the exchange contribution equals $\theta_{W,ex} = \theta_W - \theta_{W,dip} = -9.537$ K.

Table 2. Calculated and measured (in brackets) crystal field energies (cm^{-1}) of the R^{3+} ions in $Tb_2Ti_2O_7$, $Dy_2Ti_2O_7$ and $Er_2Ti_2O_7$.

Tb^{3+} ($^7F_6$)		Tb^{3+} ($^7F_5$)		Dy^{3+} ($^6H_{15/2}$)		Er^{3+} ($^4I_{15/2}$)	
E	0	E	2067.7 (2068.6[a])	Γ_{56}	0	Γ_4	0
E	11.5 (12.1[a])	A_2	2112.7 (2114.9[a])	Γ_4	194	Γ_{56}	51.7 (51.2[b])
A_2	77 (84.3[a])	E	2209.6 (2207.4[a])	Γ_{56}	287 (287[c])	Γ_4	58.2 (59.1[b])
A_1	119 (118.8[a])	E	2317.1 —	Γ_4	292	Γ_4	125 (123.2[b])
E	281	A_2	2373.4 (2375.2[a])	Γ_4	390	Γ_4	411
A_2	319	E	2481.4 —	Γ_4	592	Γ_{56}	429
A_1	322	A_1	2545.8 (2565.2[a])	Γ_4	665	Γ_4	466
E	438			Γ_{56}	682	Γ_{56}	696
A_1	510						

[a] Reference [38]. [b] Reference [50, 51]. [c] Reference [9, 39].

Using equation (24), we obtain $\lambda_{is} = -0.112$ T/μ_B, the corresponding exchange coupling constant $J/k_B = -0.306$ K is close to the value -0.32 K obtained earlier from the analysis of magnetization measurements in [37]. The specific feature of the Gd^{3+} ions revealed from calculations is the change of the sign of the magnetic anisotropy (from the easy plane to the easy axis) at low temperatures due to strong renormalization of the single ion susceptibilities (see inset (*b*) in figure 1). This effect needs experimental verification. It should be noted that the predicted change of sign of the magnetic anisotropy in $Gd_2Ti_2O_7$ as compared with the single ion planar magnetic anisotropy of impurity Gd^{3+} ions in $Y_2Ti_2O_7$ may play an essential role in the formation of unconventional magnetic structure in gadolinium titanate [2].

4.2. $Tb_2Ti_2O_7$

We calculated single ion susceptibilities of the $Tb^{3+}(4f^8)$ ions in $Tb_2Ti_2O_7$ using a slightly corrected set of CFP (table 1) presented earlier in [28]. Computed crystal field energies for the two lower multiplets of the Tb^{3+} ion agree well with the data obtained from neutron and Raman scattering measurements (see table 2) [9, 15, 38]. Note that there is an essential mixing of ^7F_J multiplets in the crystal field, and we have used the total basis of 3003 states of the $4f^8$ configuration in the calculations of the crystal field energies and corresponding wavefunctions. The calculated $g_\parallel$-factors of the ground and the first excited non-Kramers doublets equal 11.07 and 14.16, respectively. It is interesting to note that it is not necessary to change drastically this set of CFP (in particular, to change the sign of B_0^6 [15]) when considering magnetic properties and the energy spectrum of the Tb^{3+} ions in the closely related compound $Tb_2Sn_2O_7$. According to calculations of the CFP for $Tb_2Sn_2O_7$ in the framework of the exchange charge model, B_0^4 and B_0^6 decrease and the modulus of B_3^4 increases relative to the corresponding CFP for $Tb_2Ti_2O_7$, and parameters B_3^6 and B_6^6 are almost the same. The obtained set of CFP (see table 1) brings approximately the same energies of the lower four energy levels as in $Tb_2Ti_2O_7$ but with the repositioned ground and first excited doublets ($g_\parallel$ equals 13.5 and 10.5, respectively).

The calculated single ion susceptibilities differ remarkably at low temperatures from the site susceptibilities measured in [27] (figure 2, inset (*b*)). Renormalization due to the magnetic dipole–dipole interactions enhances the differences. The calculated site susceptibilities (18) and (19) match satisfactorily the experimental data at temperatures $T > 5$ K when introducing anisotropic exchange interactions with the coupling constants $\lambda_\parallel = -0.079$ T/μ_B and $\lambda_\perp = \lambda_{\perp,1} = \lambda_{\perp,2} = -0.06$ T/μ_B. We have used the demagnetizing factor $N = 1.92$ in our calculations, and relatively small uncertainties of the values of coupling constants may be expected because the shape of single crystals used in the neutron scattering experiments has not been mentioned in [27]. Also, it should be noted that magnetic moments of the Tb^{3+} ions have been measured in an external magnetic field large enough (1 T) to induce remarkable magnetoelastic effects which are not accounted for in calculations. The curves in the inset (*b*) in figure 2 correspond to the calculated components of Tb^{3+} magnetic moments in the magnetic field $B = 1$ T applied along the C_4 symmetry axis. The measured temperature dependence of the bulk susceptibility of the single crystal at temperatures $T > 2$ K is well described by expression (21) when using the calculated single ion susceptibilities and the exchange coupling constants presented above (see figure 2).

4.3. $Dy_2Ti_2O_7$

We cannot determine the CFP for $Dy_2Ti_2O_7$ unambiguously because there is no authentic experimental identification of any excited crystal field level of the Dy^{3+} ions with the ground $4f^9$ configuration except, maybe, a level at the energy of 287 cm^{-1} [9, 39]. The set of CFP used in our calculations (see table 1) was obtained by interpolation of the data for the $4f^8$ ($Tb_2Ti_2O_7$) and $4f^{10}$($Ho_2Ti_2O_7$) configurations with additional corrections to fit the crystal field excitation mentioned above. The calculated energies of the crystal field sublevels of the ground multiplet $^6H_{15/2}$ are given in table 2. The obtained energies of the lower excited states do not contradict the activation energies for the magnetic relaxation (188 and 282 cm^{-1}) determined in [40, 41]. The lower value of the activation energy (145 cm^{-1}) that has been determined from muon spin relaxation (μSR) measurements [42] may be a result of local perturbations of the crystal fields at the dysprosium sites nearest to the trapped muons.

The ground state of the Dy^{3+} ion is an Ising type doublet with g-factors $g_\parallel = 19.09$ and $g_\perp = 0$ well separated by a gap $\delta E = 280$ K from excited energy levels. The additional adjustable parameter, the orbital reduction factor k [43], with the reasonable final value of $k = 0.95$ was introduced into

the magnetic moment operator $\boldsymbol{m} = \mu_B \sum (k\boldsymbol{l} + 2\boldsymbol{s})$ to fit the measured bulk susceptibility at temperatures $T > 250$ K. The single ion susceptibilities at low temperatures ($k_B T \ll \delta E$) are $\chi_\parallel^s = (g_\parallel \mu_B)^2/4k_B T + \chi_\parallel^V$ and $\chi_\perp^s = \chi_\perp^V$, where $\chi_\parallel^V < 0.002\ \mu_B\ T^{-1}$ and $\chi_\perp^V = 0.0258 \mu_B\ T^{-1}$ are the corresponding Van Vleck susceptibilities. Thus, for temperatures $T < 50$ K, we can neglect the Van Vleck terms and describe the bulk susceptibility by the Curie–Weiss expression with the Weiss temperature (see equations (20) and (21))

$$\theta_W = 2\frac{J_{nn}}{k_B} + \frac{(g_\parallel \mu_B)^2}{6k_B}\left[2q - p + \frac{8\pi}{3v}(1-N)\right], \qquad (25)$$

where $J_{nn} = (2\lambda_\parallel - \lambda_{\perp,1})(g_\parallel \mu_B/2)^2/3$ is the exchange energy for the two nearest neighbor ions introduced earlier in [44]. The dipolar contribution (the second term on the right-hand side in expression (25)), $\theta_{W,dip} = 4\pi(g_\parallel \mu_B)^2(3.7607 - N)/9vk_B$, where $0 \leqslant N \leqslant 3$, is always positive and competes with the contribution from the antiferromagnetic ($J_{nn} < 0$) exchange interaction. Using the results of our measurements (see figure 3), we determined $\theta_W = 0.7$ K. This value agrees with the data for polycrystalline samples [8] but is less than the values, 1.16–1.31 K, obtained in [19] for a single crystal with $N = 1.2$. Substituting the known value of the demagnetizing factor, the measured θ_W and the calculated g-factor $g_\parallel$ into the expression (25), we estimated the exchange energy $J_{nn}/k_B = -1.66$ K. However, from fitting of the measured temperature dependence of the bulk susceptibility in the larger range of temperatures, 10 K $< T <$ 300 K, we obtained the exchange coupling constants $\lambda_\parallel = -0.044\ T/\mu_B$, $\lambda_{\perp,1} = \lambda_{\perp,2} = -0.016\ T/\mu_B$, and the corresponding slightly lower value of the exchange energy $J_{nn}/k_B = -1.465$ K. The obtained ratio $J_{nn}/D_{nn} = -0.71$, where $D_{nn} = (5/3)(g_\parallel \mu_B/2)^2/r_{nn}^3$ is the energy of the dipole–dipole interaction between the nearest neighbor ions at low temperatures ($D_{nn}/k_B = 2.06$ K), belongs to a region of the phase diagram presented in [44] that corresponds to the spin ice behavior.

4.4. $Ho_2Ti_2O_7$

The Ho^{3+} and Dy^{3+} ions in titanate pyrochlores have very similar magnetic properties. Parameters of the crystal field Hamiltonian operating in the space of states of the ground $^5I_8$ multiplet of the Ho^{3+} ions were determined earlier in [28, 45]. In the current work, we started from these parameters and obtained a more accurate parameter set (see table 1) from the fitting procedure based on computations of the thermal averages (9) and (10) with the effective Hamiltonian (2) operating in the total space of 1001 states of the $4f^{10}$ configuration. The calculated crystal field energies for several lower multiplets are presented in table 3. We can describe satisfactorily the neutron scattering measurements [11] and assign most of the spectral lines in the optical absorption spectra [46] in the corresponding frequency windows to transitions between the ground state and the crystal field sublevels of the $^5I_7$, $^5I_6$, $^5S_2$, $^5F_4$ multiplets (see table 3). However, the observed optical spectra contain a number of extra lines of unknown nature [9, 46]. The ground state of the Ho^{3+} ion, well separated by a gap $\delta E = 240$ K from excited energy levels, is the non-Kramers doublet with the calculated g-factors $g_\parallel = 19.086$ and $g_\perp = 0$ (the orbital reduction factor $k = 0.975$ was introduced to fit the measured bulk susceptibility at room temperature). The calculated Van Vleck contributions to the low temperature single ion susceptibilities are $\chi_\parallel^V = 0.009\ \mu_B\ T^{-1}$ and $\chi_\perp^V = 0.0194\ \mu_B\ T^{-1}$. Neglecting these terms and using the measured value of the Weiss temperature $\theta_W = 1.49$ K (corresponding to the temperature range from 20 to 50 K), we obtain the exchange energy $J_{nn}/k_B = -1.32$ K from the expression (25). It should be noted that, as follows from direct calculations, the magnetic hyperfine interaction in the Ho^{3+} ion (the nuclear spin $I = 7/2$) practically does not contribute to the dc-susceptibility at temperatures $T > 1$ K.

From the simultaneous fitting of the bulk (figure 4) and site susceptibilities (measured in the field $B = 1$ T in [27], see inset (b) in figure 4), we obtained the exchange coupling constants $\lambda_\parallel = -0.0275\ T/\mu_B$, $\lambda_{\perp,1} = \lambda_{\perp,2} = -0.0023\ T/\mu_B$, and the corresponding value of the nearest neighbor exchange energy $J_{nn}/k_B = -1.02$ K. So, similarly to the results obtained for the dysprosium titanate, the detailed analysis of the susceptibility of $Ho_2Ti_2O_7$ in the wide temperature range brings somewhat lower (by 12–22%) exchange energy as compared with the estimations from the Weiss temperature (25). The obtained

Table 3. Crystal field energies (cm^{-1}) of the Ho^{3+} ions in $Ho_2Ti_2O_7$.

$^{2S+1}L_J$	Γ	Theory	Exper. [46]	$^{2S+1}L_J$	Γ	Theory	Exper. [46]
$^5I_8$	E	0	0	$^5F_5$	A_2	15 548	15 558
	A_2	167.3			E	15 595	
	E	176.5	177[a]		E	15 598	
	E	210.2	210[a]		E	15 765	15 757
	A_1	219.9	225		A_2	15 871	
	E	468.7	476[a]		E	15 890	15 892
	A_1	546.4	540		A_1	15 892	
	A_2	561.2					
	E	565.5	568	$^5S_2 + {}^5F_4$			
	E	615.8	621[a]		E	18 567	18 572
	A_1	643.8	632		E	18 623	
					A_1	18 645	18 635
$^5I_7$	E	5245	5246		A_2	18 714	18 714
	A_2	5353	5357		E	18 741	18 742
	E	5375	5384		E	18 783	18 766
	E	5408	5412		A_1	18 837	18 811
	A_1	5422			E	18 869	18 859
	A_2	5437	5436		A_1	18 875	18 884
	A_1	5445	5455				
	A_2	5473	5488	$^5F_2$	E	21 214	
	E	5498	5502		E	21 332	21 341
	E	5518			A_1	21 383	21 377
$^5I_6$	A_1	8789	8779	$^3K_8$	A_1	21 430	
	A_2	8795			A_2	21 471	21 454
	E	8855	8840		E	21 481	
	A_1	8856			E	21 492	
	E	8891	8902		A_1	21 495	
	E	8926	8930		E	21 544	
	A_1	8955	8950		A_1	21 641	
	E	9009	9002		E	21 643	21 649
	A_2	9044	9050		E	21 663	21 670
					A_2	21 672	
					E	21 737	21 729

[a] Reference [11].

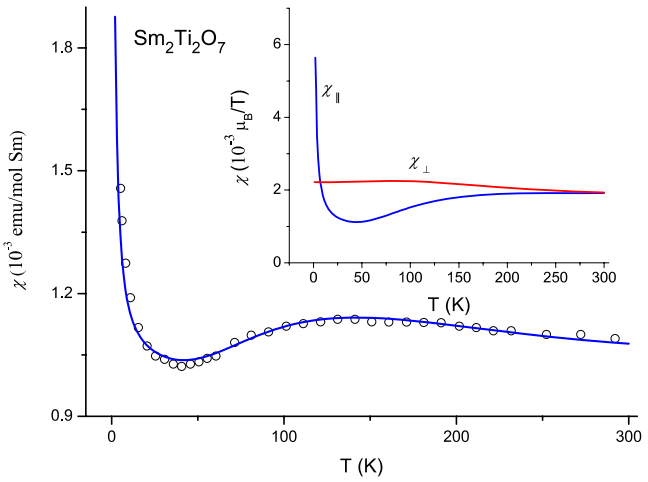

Figure 5. Calculated (solid curve) bulk susceptibility of $Sm_2Ti_2O_7$ (symbols—experimental data digitized from [3]). Inset—calculated components of the single ion susceptibility tensor.

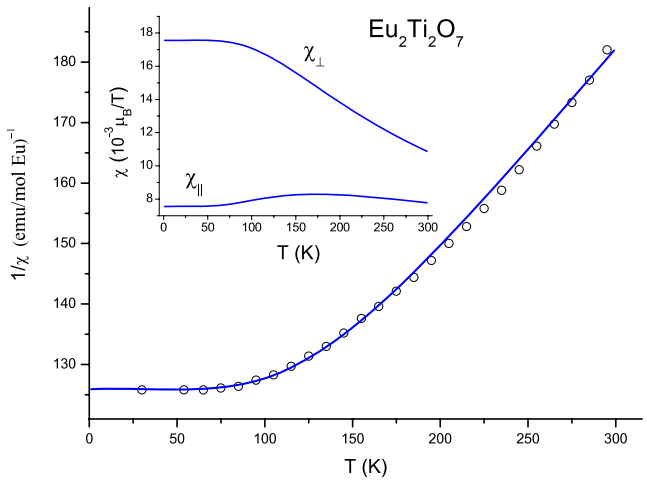

Figure 6. Calculated inverse bulk susceptibility of $Eu_2Ti_2O_7$ ($N = 1$, $\lambda_\parallel = \lambda_\perp = 0$, solid curve). Symbols—experimental data digitized from [4]. Inset: calculated site susceptibilities.

ratio $J_{nn}/D_{nn} = -0.49$ ($D_{nn}/k_B = 2.07$ K) is well above the boundary value, -0.91, on the phase diagram presented in [44], and corresponds to the spin ice behavior.

4.5. $Sm_2Ti_2O_7$

The obtained set of CFP (see table 1) allows us to reproduce satisfactorily the temperature dependence of the bulk susceptibility of $Sm_2Ti_2O_7$ measured in the temperature range from 5 to 300 K in [3] (see figure 5). The lowest multiplet $^6H_{5/2}$ of the $Sm^{3+}(4f^5)$ ion is split by the trigonal crystal field into three Kramers doublets with the following energies and g-factors: 0 (Γ_{56}, $g_\parallel = 0.24$, $g_\perp = 0$), 172.4 cm^{-1} (Γ_4, $g_\parallel = 1.36$, $g_\perp = 0.78$), 212.7 cm^{-1} (Γ_4, $g_\parallel = 1.7$, $g_\perp = 1.15$). At temperatures higher than 1 K, the effect of magnetic interactions between the Sm^{3+} ions on the dc-susceptibility is negligible due to the large gap between the excited states and the ground state with the very small g-factor. In this case the single ion susceptibilities are not renormalized (see inset in figure 5), and the bulk susceptibility does not depend on the sample shape. The pronounced broad maximum of the bulk susceptibility centered at $T = 140$ K is caused by thermal excitations of the excited states with large g-factors as compared to the g-factor of the ground state. The crystal field energies presented above do not agree with frequencies of the extra modes (87, 132, 158, 270 cm^{-1}) observed in the low temperature Raman spectrum of $Sm_2Ti_2O_7$ and ascribed to electronic excitations (crystal field modes) [3]. In any case, only two crystal field modes with frequencies less than 10^3 cm^{-1} may be observed, and it is more likely that the observed extra modes correspond to IR active phonons (see [47]) which become Raman active due to crystal inhomogeneities.

4.6. $Eu_2Ti_2O_7$

The Eu^{3+} ion has the singlet ground state $^7F_0(A_1)$, and at low temperatures ($T < 80$ K) the bulk susceptibility, as reported in [4], contains the temperature independent Van Vleck contribution only. At higher temperatures, the susceptibility decreases due to increasing populations of crystal field sublevels of the first excited $^7F_1$ multiplet. Because the relatively low lying charge transfer band [48] affects the crystal field energies of the ground $4f^6$ electronic configuration, a detailed analysis of the energy level pattern of the Eu^{3+} ion is a complicated problem that goes beyond the scope of the present work. We succeeded in fitting the temperature dependence of the susceptibility (see figure 6) using the free ion parameters given in [49] for the Eu^{3+} ions in Lu_2O_3 and the set of CFP presented in table 1, and introducing the orbital reduction factor $k = 0.905$. It should be noted that, due to different signs of the orbital and spin moments in the states belonging to lower multiplets of the Eu^{3+} ion, reduction of the orbital magnetic moment leads to enhancement of the susceptibility of the Eu^{3+} ion in contrast to the case of heavier ions from the second half of the lanthanide series with the same signs of the orbital and spin moments in the ground state.

4.7. $Er_2Ti_2O_7$

The set of CFP for the $Er^{3+}(4f^{11})$ ions (see table 1) was obtained from fitting the theoretical results to the temperature dependence of the site susceptibilities presented in [27] and to the energies of the three lower crystal field sublevels of the ground multiplet $^4I_{15/2}$, as determined in inelastic neutron scattering experiments [50, 51]. The calculated and measured energies of the crystal field sublevels are compared in table 2. Similarly to the procedure employed above, the orbital reduction factor, $k = 0.98$, was introduced when calculating the single ion susceptibilities. The calculated g-factors of the ground state doublet $g_\perp = 6.546$, $g_\parallel = 3.01$ agree with the measured saturated moment 3.25 μ_B of the Er^{3+} ions in the magnetically ordered state [52]. The single ion susceptibilities differ significantly from the experimental data at temperatures below 15 K, the distinctions between the calculated and measured longitudinal (transversal)

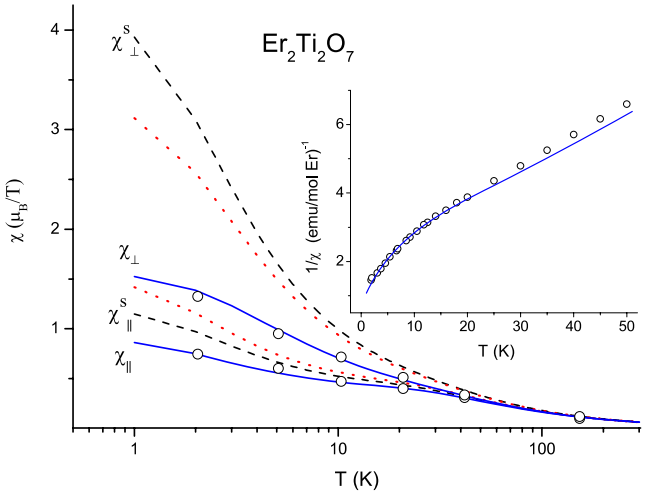

Figure 7. Measured (symbols) [27] and calculated components of the site susceptibility tensor of $Er_2Ti_2O_7$ (dotted curves—single ion susceptibilities in the crystal field, dashed curves and solid curves—renormalized susceptibilities due to dipole and dipole + exchange interactions, respectively). Inset: the calculated ($N = 1$, solid curve) inverse bulk susceptibility (symbols: experimental data for the polycrystalline sample digitized from [8]).

susceptibilities increase (decrease) when accounting for the dipole–dipole interactions (see figure 7). The renormalized site susceptibilities agree with the experimental data when introducing the anisotropic exchange interaction with the coupling constants $\lambda_\parallel = -0.0218$ T/μ_B and $\lambda_{\perp,1} = \lambda_{\perp,2} = -0.0741$ T/μ_B. At high temperatures ($T > 20$ K), the calculated bulk susceptibility can be formally described by the Curie–Weiss law with $\theta_W = -20$ K, which is close to the value of -22 K obtained in [8]. At lower temperatures results of calculations for a spherical sample match the measured susceptibility of a polycrystalline sample [8] very well (see inset in figure 7).

4.8. $Yb_2Ti_2O_7$

Our attempts to describe the crystal field energies of the $Yb^{3+}(4f^{13})$ ions in $Yb_2Ti_2O_7$ determined from optical spectra [28] and the recently observed temperature dependence of the longitudinal site susceptibility $\chi_\parallel$ [27, 29] by making use of a single set of CFP have failed. The $g_\parallel$ value for the ground doublet determined from the experimental results presented in [27, 29] is remarkably different from the previously published one (2.25 versus 1.79) for the impurity Yb^{3+} ions in $Y_2Ti_2O_7$ [25]. Also, to reproduce the variation of $\chi_\parallel$ with temperature, it is necessary to introduce an exchange coupling constant $\lambda_\parallel$ that should be about an order of magnitude larger than in other rare earth titanate pyrochlores and, in particular, than the inter-ionic coupling constant determined from the magnetization measurements in $Yb_2Ti_2O_7$ [25]. It seems obvious that additional experimental studies of optical and magnetic properties of $Yb_2Ti_2O_7$ are necessary to collect mutually consistent data in order to facilitate a subsequent theoretical analysis.

5. Summary

We have derived the expressions for the site and bulk magnetic susceptibilities of the pyrochlore lattice in the framework of the mean field approximation taking into account the main (dipole–dipole and exchange) interactions between paramagnetic ions. These expressions allowed us to analyze the experimental data obtained in the present work and the data published earlier and to extract information about the crystal fields and anisotropic exchange coupling constants in different rare earth titanates with the pyrochlore structure. In particular, we have analyzed very interesting and unique data on temperature dependencies of site susceptibilities in $R_2Ti_2O_7$ (R = Ho, Tb, Er and Yb) obtained by Cao *et al* [27] from polarized neutron diffraction measurements. These data were interpreted in [27] in the framework of the phenomenological model based on the introduction of the anisotropic diagonal molecular field tensor. The principal shortcoming of this model is a neglect of an off-diagonal element of the molecular field tensor (see equations (13)–(17) above, the off-diagonal element $\sqrt{2}D$ and the diagonal elements A and F have the same order of magnitude). Our approach allows one to obtain more reliable estimations of the molecular field parameters and to compare explicitly corresponding contributions from the dipole–dipole and exchange interactions.

Determination of the reliable CFP for different rare earth ions in pyrochlores is a challenging problem due to very limited information about the crystal field splittings of the ground and excited multiplets. Zero-phonon electric dipole transitions within the manifold of the $4f^N$ configuration energy levels are strictly forbidden, intensities of zero-phonon magnetic dipole transitions are negligible or at best comparable to intensities of electron-vibrational electric dipole transitions which involve creation or annihilation of phonons. Also, even a very small concentration of defect (extrinsic) optical centers at the sites with broken inversion symmetry, where electric dipole transitions are allowed, can significantly complicate the interpretation of optical spectra [28]. In the present work, we have demonstrated that the measured temperature dependence of the bulk and site susceptibilities as well as most of the existing data on the crystal field energies of rare earth ions in titanate pyrochlores can be successfully described by making use of CFP which are approximately constant or vary monotonously along the lanthanide series (see table 1). We have shown that only minor corrections of the previously obtained CFP for Tb and Ho titanates [28] allow us to describe satisfactorily new experimental data (frequencies of optical transitions and the temperature dependence of the bulk and site susceptibilities). The set of CFP for $Sm_2Ti_2O_7$ is presented for the first time. We have also obtained in the current work new sets of CFP for Eu, Dy and Er titanates which satisfy the general trends of CFP variations along the lanthanide series. The unconventional behavior of the parameter B_0^2, which increases with the diminishing radius of the unfilled 4f shell, may be caused by a specific rearrangement of the nearest surroundings of rare earth ions in titanate pyrochlores [1, 28]. The values of the CFP presented in [27] for Tb, Ho, Er titanates agree qualitatively with our results but bring underestimated

Table 4. Constants of the isotropic ($\lambda_{is} = (\lambda_{\parallel} + \lambda_{\perp,1} + \lambda_{\perp,2})/3$) and anisotropic ($\lambda_{anis} = \lambda_{\parallel} - \lambda_{\perp,1}$) exchange interactions in $R_2Ti_2O_7$ (in units of T/μ_B).

	Gd	Tb	Dy	Ho	Er
λ_{is}	−0.112	−0.0663	−0.0253	−0.0107	−0.0567
λ_{anis}	0	−0.0190	−0.0280	−0.0252	0.0523

crystal field splittings. The CFP obtained in [4, 22, 24, 53] for Eu, Ho, Er and Dy titanates vary randomly from one compound to another and cannot be related to any physical model of a crystal field. The set of CFP obtained in our previous work [28] for Yb titanate is consistent with the measured temperature dependence of the bulk and transversal site susceptibilities, but contradicts the experimental data [27] on the longitudinal site susceptibility. The problem of a self-consistent description of the optical and magnetic properties of $Yb_2Ti_2O_7$ remains unsolved.

There are evident distinctions between the experimental data and the calculated bulk and site susceptibilities of $Gd_2Ti_2O_7$, $Dy_2Ti_2O_7$ and $Ho_2Ti_2O_7$ at low temperatures ($T < 10$ K) (see figures 1, 3 and 4). In these systems rare earth ions have large magnetic moments, and the calculated susceptibilities are overestimated due to neglect of fluctuations of the magnetic moments which destroy ferromagnetic dipole–dipole correlations. Note that in the present work we have employed the simplest (single site) mean field approach and have not independently varied the transversal exchange coupling constants $\lambda_{\perp,1}$ and $\lambda_{\perp,2}$. However, the possibility to use one more degree of freedom in the fitting procedure may be of importance in the analysis of future more detailed experimental data on the site susceptibilities. We expect that the agreement between the theoretical results and the experimental data can further be improved by introducing a cluster (single tetrahedron) approximation [54] that should account for magnetic dipole interactions along with exchange interactions.

We believe that the obtained sets of CFP and exchange coupling constants collected in table 4 may serve as a basis for the analysis of future experiments on the field and temperature dependence of the magnetization, the interpretation of optical spectra and for calculations of the electron–phonon coupling constants in rare earth pyrochlores.

Acknowledgments

BZM and ARZ are grateful to the Russian Foundation for Basic Research for partial support of this work under grant N09-02-00930. The authors would like to thank A Revcolevschi for facilitating the single crystal growth and TTM Palstra for facilitating use of the SQUID magnetometer.

References

[1] Lian J, Chen J, Wang L M, Ewing R C, Farmer J M, Boatner L A and Helean K B 2003 *Phys. Rev.* B **68** 134107
[2] Gardner J S, Gingras M J P and Greedan J E 2010 *Rev. Mod. Phys.* **82** 53
[3] Singh S, Saha S, Dhar S K, Suryanarayanan R, Sood A K and Revcolevschi A 2008 *Phys. Rev.* B **77** 054408
[4] Dasgupta P, Jana Y M, Nag Chattopadhyay A, Nigashinaka R, Maeno Y and Ghosh D 2007 *J. Phys. Chem. Solids* **68** 347
[5] Raju N P, Dion M, Gingras M J P, Mason T E and Greedan J E 1999 *Phys. Rev.* B **59** 14489
[6] Ramirez A P, Shastry B S, Hayashi A, Krajewski J J, Huse D A and Cava R J 2002 *Phys. Rev. Lett.* **89** 067202
[7] Bonville P, Hodges J A, Ocio M, Sanchez J P, Vulliet P, Sosin S and Braithwaite D 2003 *J. Phys.: Condens. Matter* **15** 7777
[8] Bramwell S T, Field M N, Harris M J and Parkin I P 2000 *J. Phys.: Condens. Matter* **12** 483
[9] Lummen T T A, Handayani I P, Donker M C, Fausti D, Dhalenne G, Berthet P, Revcolevschi A and van Loosdrecht P H M 2008 *Phys. Rev.* B **77** 214310
[10] Luo G, Hess S T and Corruccini L R 2001 *Phys. Lett.* A **291** 306
[11] Siddharthan R, Shastry B S, Ramirez A P, Hayashi A, Cava R J and Rosenkranz S 1999 *Phys. Rev. Lett.* **83** 1854
[12] Gingras M J P, den Hertog B C, Faucher M, Gardner J S, Dunsiger S R, Chang L J, Gaulin B D, Raju N P and Greedan J E 2000 *Phys. Rev.* B **62** 6496
[13] Gardner J S, Dunsiger S R, Gaulin B D, Gingras M J P, Greedan J E, Kiefl R F, Lumsden M D, MacFarlane W A, Raju N P, Sonier J E, Swainson I and Tun Z 1999 *Phys. Rev. Lett.* **82** 1012
[14] Alexandrov I V, Lidskii B, Mamsurova L G, Neigauz M G, Pigalskii K S, Pukhov K K, Trusevich N G and Scherbakova L G 1985 *Sov. Phys.—JETP* **62** 1287
[15] Mirebeau I, Bonville P and Hennion M 2007 *Phys. Rev.* B **76** 184436
[16] Gardner J S, Ehlers J, Bramwell S T and Gaulin B D 2004 *J. Phys.: Condens. Matter* **16** S643
[17] Townsend M G and Crossley W A 1968 *J. Phys. Chem. Solids* **29** 593
[18] Blote H W J, Wielinga R F and Huiskamp H 1969 *Physica* **43** 549
[19] Fukazawa H, Melko R G, Higashinaka R, Maeno Y and Gingras M J P 2002 *Phys. Rev.* B **65** 054410
[20] Mamsurova L G, Pukhov K K, Trusevich N G and Scherbakova L G 1985 *Sov. Phys.—Solid State* **27** 1214
[21] Matsuhira K, Hinatsu Y, Tenya K and Sakakibara T 2000 *J. Phys.: Condens. Matter* **12** L649
[22] Jana Y M and Ghosh D 2000 *Phys. Rev.* B **61** 9657
[23] Cornelius A L and Gardner J S 2001 *Phys. Rev.* B **64** 060406
[24] Dasgupta P, Jana Y and Ghosh D 2006 *Solid State Commun.* **139** 424
[25] Hodges J A, Bonville P, Forget A, Rams M, Krolas K and Dhalenne G 2001 *J. Phys.: Condens. Matter* **13** 9301
[26] Yasui Y, Soda M, Iikubo S, Ito M, Sato M, Hamaguchi N, Matsushita T, Wada N, Takeuchi T, Aso N and Kakura K 2003 *J. Phys. Soc. Japan* **72** 3014
[27] Cao H B, Gukasov A, Mirebeau I, Bonville P, Decorse C and Dhalenne G 2009 *Phys. Rev. Lett.* **103** 056402
[28] Malkin B Z, Zakirov A R, Popova M N, Klimin S A, Chukalina E P, Antic-Fidancev E, Goldner Ph, Aschehoug P and Dhalenne G 2004 *Phys. Rev.* B **70** 075112
[29] Cao H B, Gukasov A, Mirebeau I and Bonville P 2009 *J. Phys.: Condens. Matter* **21** 492202
[30] Van Vleck J H 1932 *Theory of Electric and Magnetic Susceptibilities* (Oxford: Oxford University Press)
[31] Schechter M and Stamp P C E 2005 *Phys. Rev. Lett.* **95** 267208
[32] Elliott R J, Harley R T, Hayes W and Smith S R P 1972 *Proc. R. Soc.* A **328** 217
[33] Sato M and Ishii Y 1989 *J. Appl. Phys.* **66** 983
[34] Osborn J A 1945 *Phys. Rev.* **67** 351
[35] Carnall W T, Goodman G L, Rajnak K and Rana R S 1989 *J. Chem. Phys.* **90** 3443

[36] Glazkov V N, Zhitomirsky M E, Smirnov A I, Krug fon Nidda H A, Loidl A, Marin C and Sanchez J P 2005 *Phys. Rev.* B **72** 020409R
[37] Sosin S S, Prozorova L A, Smirnov A I, Bonville P, Jasmin-Le Bras G and Petrenko O A 2007 arXiv:0709.4379 [cond-mat]
[38] Maczka M, Sanjuán M L, Fuentes A F, Hermanowicz K and Hanuza J 2008 *Phys. Rev.* B **78** 134420
[39] Maczka M, Sanjuán M L, Fuentes A F, Macalik L, Hanuza J, Matsuhira K and Hiroi Z 2009 *Phys. Rev.* B **79** 214437
[40] Sutter J P, Tsutsui S, Higashinaka R, Maeno Y, Leupold O and Baron A Q R 2007 *Phys. Rev.* B **75** 140402(R)
[41] Kitagawa K, Higashinaka R, Ishida K, Maeno Y and Takigawa M 2008 *Phys. Rev.* B **77** 214403
[42] Lago J, Blundell S J and Baines C 2007 *J. Phys.: Condens. Matter* **19** 326210
[43] Abragam A and Bleaney B 1970 *Electron Paramagnetic Resonance of Transitiuon Ions* (Oxford: Clarendon)
[44] den Hartog B C and Gingras M J P 2000 *Phys. Rev. Lett.* **84** 3430
[45] Rosenkranz S, Ramirez A P, Hayashi A, Cava R J, Siddharthan R and Shastry B S 2000 *J. Appl. Phys.* **87** 5914
[46] Macalik L, Maczka M, Solarz P, Fuentes A F, Matsuhira K and Hiroi Z 2009 *Opt. Mater.* **31** 790
[47] Bi C Z, Ma J Y, Zhao B R, Tang Z, Yin D, Li C Z, Yao D Z, Shi J and Qiu X G 2005 *J. Phys.: Condens. Matter* **17** 5225
[48] Pidol L, Viana B, Galtayries A and Dorenbos P 2005 *Phys. Rev.* B **72** 125110
[49] Karbowiak M, Zych E and Hölsä J 2003 *J. Phys.: Condens. Matter* **15** 2169
[50] Champion J D M, Harris M J, Holdsworth P C W, Wills A S, Balakrishnan G, Bramwell S T, Cizmar E, Fennell T, Gardner J S, Lago J, McMorrow D F, Orendac M, Orendacova A, Paul D McK, Smith R I, Telling M T F and Wildes A 2003 *Phys. Rev.* B **68** 020401(R)
[51] Gardner J S and Ehlers G 2009 *J. Phys.: Condens. Matter* **21** 436004
[52] Poole A, Wills A S and Lelievre-Berna E 2007 *J. Phys.: Condens. Matter* **19** 452201
[53] Jana Y M, Sengupta A and Ghosh D 2002 *J. Magn. Magn. Mater.* **248** 7
[54] Garcia-Adeva A J and Huber D L 2000 *Phys. Rev. Lett.* **85** 4598